

Article

Enhanced Extracellular Synthesis of Gold Nanoparticles by Soluble Extracts from *Escherichia coli* Transformed with *Rhizobium tropici* Phytochelatin Synthase Gene

Qunying Yuan ^{1,*} , Manjula Bomma ¹ and Zhigang Xiao ² 

¹ Department of Biological and Environmental Science, Alabama A&M University, Normal, AL 35762, USA; manjula.bomma@aamu.edu

² Department of Electrical Engineering and Computer Science, Alabama A&M University, Normal, AL 35762, USA; zhigang.xiao@aamu.edu

* Correspondence: qunying.yuan@aamu.edu; Tel.: +1-256-372-4241

Abstract: Phytochelatins, the enzymatic products of phytochelatin synthase, play a principal role in protecting the plants from heavy metal and metalloids toxicity due to their ability to scavenge metal ions. In the present study, we investigated the capacity of soluble intracellular extracts from *E. coli* cells expressing *R. tropici* phytochelatin synthase to synthesize gold nanoparticles. We discovered that the reaction mediated by soluble extracts from the recombinant *E. coli* cells had a higher yield of gold nanoparticles, compared to that from the control cells. The compositional and morphological properties of the gold nanoparticles synthesized by the intracellular extracts from recombinant cells and control cells were similar. In addition, this extracellular nanoparticle synthesis method produced purer gold nanoparticles, avoiding the isolation of nanoparticles from cellular debris when whole cells are used to synthesize nanoparticles. Our results suggested that phytochelatins can improve the efficiency of gold nanoparticle synthesis mediated by bacterial soluble intracellular extracts, and the potential of extracellular nanoparticle synthesis platform for the production of nanoparticles in large quantity and pure form is worth further investigation.

Keywords: gold nanoparticles; extracellular nanoparticle synthesis; recombinant *Escherichia coli*; phytochelatin synthase; phytochelatins



Citation: Yuan, Q.; Bomma, M.; Xiao, Z. Enhanced Extracellular Synthesis of Gold Nanoparticles by Soluble Extracts from *Escherichia coli* Transformed with *Rhizobium tropici* Phytochelatin Synthase Gene. *Metals* **2021**, *11*, 472. <https://doi.org/10.3390/met11030472>

Academic Editor: Marco Martino

Received: 24 January 2021

Accepted: 10 March 2021

Published: 12 March 2021

Publisher's Note: MDPI stays neutral with regard to jurisdictional claims in published maps and institutional affiliations.



Copyright: © 2021 by the authors. Licensee MDPI, Basel, Switzerland. This article is an open access article distributed under the terms and conditions of the Creative Commons Attribution (CC BY) license (<https://creativecommons.org/licenses/by/4.0/>).

1. Introduction

Nanoparticles have diverse applications in various fields, including, but not limited to, serving as carriers for drug delivery, new materials for pathogen detection or food preservation, prevention and remediation of heavy metal contaminants, as well as generation of renewable energy production [1]. Microbial synthesis of nanoparticles is increasingly becoming the focus for the development of new methods for nanoparticle production due to its low cost, environmental friendliness and potential to upgrade for large scale production. Microorganisms, such as bacteria and fungi, possess metal ion regulators, transporters, ligands, metal-dependent reductases, metal binding and reducing agents that are natural and essential for the process of biological synthesis of nanoparticles, from reducing metal ions into elemental metal, to further binding, capping and stabilizing the metal elements as nanoparticles [1–3].

We are interested in exploring the contribution of a group of metal-binding peptides, phytochelatins, to the bacteria nanoparticle synthesis. The production of phytochelatins is catalyzed by phytochelatin synthase in plants, and recently also found in prokaryotes [4–7]. The role of phytochelatins in prokaryotes is not completely elucidated, but it is well accepted that phytochelatins play a principal role in protecting plants from heavy metal and metalloids toxicity [4,5,8–12], due to the presence of clusters of cysteine residues that can bind to metal ions. The phytochelatins are short peptides that have a general structure of (γ -Glu-Cys) n -Gly, where n is usually no more than 5, but can be between 2 and

11 [4,5,11]. The thiols of cysteine residues in phytochelatins interact with metals with high affinity and form the phytochelatin-metal complex during detoxification of metals and metalloids in plants [4,8,11]. The contribution of phytochelatins to nanoparticle synthesis has been investigated [13–15]. We also developed a recombinant *E. coli* bacterium that expresses *R. tropici* phytochelatin synthase, and discovered that overexpression of *R. tropici* phytochelatin synthase in *E. coli* cells improved the bacterial heavy metal resistance, and increased yield of selenium nanoparticles when whole cells were used to synthesize nanoparticles [16]. Nevertheless, one challenge associated with whole cell nanoparticle synthesis in our previous studies was the isolation of nanoparticles from cellular debris to obtain pure nanoparticles. Thus, one goal of the present study was to tackle this issue by utilizing the intracellular soluble components from the *E. coli* cells as reaction media for nanoparticle synthesis; additionally, we further examined the impacts of phytochelatins on nanoparticle production via the extracellular nanoparticle synthesis method.

Nanoparticle synthesis mediated by soluble extracts from microorganisms have been explored [1,17–20]; however, the exact mechanisms are not well elucidated. It is generally agreed that the nanoparticles are formed through two important steps: metal or metalloid ions are first trapped on the surface or transported into the microbial cells. The trapped ions are then reduced to nanoparticles in the presence of enzymes [21]. Thus, the enzymes and functional groups of biomolecules present either in the cell walls or inside the cells are essential for the reduction of metal ions, nucleation, capping, stabilization of nanoparticles [21,22]. These agents include large molecules, such as reductases, other enzymes, proteins, cofactors and polysaccharides [18,23–29], as well as small ones, such as peptides, glucose and amino acids [19,22,29–32]. For an example, Vetchinkina et al showed that some enzymes, such as Mn-peroxidases, laccases, tyrosinases and phenol oxidase from basidiomycetes, were involved in the reduction of metal ions and the formation of the nanoparticles [18]. Particularly, Zsófia Molnár explored the role of various components of thermophilic filamentous fungi in gold nanoparticle synthesis and revealed that different cellular components (intracellular soluble molecules, components released to extracellular environment, and whole cellular lysate) were able to produce gold nanoparticles; however, the formation of nanoparticles with different sizes and nanoparticle size distributions depends on the fungi strain and experimental conditions [19]. Interestingly, they found that the size of reducing agents was less than 3 kDa, but the size of molecules that can efficiently stabilize nanoparticles was greater than 3 kDa [19].

The majority of these biological molecules are soluble and some of them are even released to the extracellular growth medium. In principle, employing the soluble intracellular extracts as a reaction medium for nanoparticle synthesis can avoid the tedious and nearly impossible isolation of nanoparticles from cellular debris. In our previous study, the recombinant *E. coli* DH5a cells that express *R. tropici* phytochelatin synthase showed increased efficiency in selenium nanoparticle synthesis [16]. We postulated that the enhanced capacity of these recombinant bacteria for nanoparticle synthesis was resulted from the increased phytochelatin production upon the overexpression of *R. tropici* phytochelatin synthase. Thus, we proposed that the soluble extracts from *E. coli* DH5a cells transformed with *R. tropici* phytochelatin synthase gene should be able to improve nanoparticle synthesis due to the increase in phytochelatin level.

Gold nanoparticles have the potential applications in diverse fields, including optics, electronics, medicine and biotechnology, due to their stable chemical properties and good biocompatibility [18,33]. Thus, we specifically evaluated how overexpression of the *R. tropici* phytochelatin synthase in *E. coli* would impact extracellular gold nanoparticle synthesis when soluble intracellular extracts are used as reaction media.

2. Materials and Methods

2.1. Determination of *R. tropici* Phytochelatin Synthase Protein Expression in Recombinant *E.*

The assembly of the *R. tropici* phytochelatin synthase gene was carried out as described by D. Marsc and Q. Yuan [16,34,35]. Glycerol stocks of *E. coli* DH5 α cells transformed

with plasmid containing the sequence-verified phytochelatin synthase gene were prepared for protein expression evaluation and nanoparticle synthesis as previously described [16]. All chemicals and reagents were purchased from Fisher Scientific (Pittsburgh, PA, USA) unless specified.

Preparation of *E. coli* DH5 α cells for determining protein expression was carried out as described in reference [16]. Cell pellets were resuspended in lysis buffer containing 50 mM Tris-HCl (pH 8), 50 mM NaCl and sonicated to break apart the cells. The whole lysate was centrifuge at 15,000 $\times g$ for 30 min to separate the soluble proteins from the cell membrane debris. Level of protein expression was examined as described in reference [16]. Briefly, 10 μ L of the supernatant was loaded to 10% SDS-PAGE gel and proteins were separated by electrophoresis. Proteins were stained with Coomassie blue staining. Gel picture was taken using Gel Doc EZ Gel Documentation System (Biorad, Hercules, CA, USA).

2.2. Synthesis of Gold Nanoparticles

The preparation of overnight culture for extracellular gold nanoparticle synthesis was carried out as described in reference [16]. The overnight cell culture was centrifuged and cells were resuspended in 100 mL of LB in the presence of carbenicillin and cultivated at 37 $^{\circ}$ C. When OD_{600nm} of control group reached around 0.8, cells were centrifuged at 4500 $\times g$ for 15 min, then the cell pellet was washed with 25 mL of 50 mM sodium phosphate buffer pH7.5 and further resuspended in 2 mL of 50 mM sodium phosphate buffer, pH7.5. Subsequently, cells were sonicated on ice for three cycles of 60 pulses at an output of 20%, with a 1-min interval between each cycle. The lysate was spun down to remove the cell debris. The soluble intracellular extract was added to 100 mL of 50 mM sodium phosphate buffer, pH7.5, containing 2 mM HAuCl₄. This cell-free reaction mix was incubated at 37 $^{\circ}$ C with continuous shake at 250 rpm for 7 days.

An additional objective of this study was to find out whether extracellular nanoparticle synthesis would facilitate the removal of cellular debris and produce purer nanoparticles, compared to the whole-cell synthesis platform. To simplify the experiments, we only chose recombinant *E. coli* cells as the source for reaction media. Whole-cell synthesis was carried out by adding HAuCl₄ to the cell culture at 2 mM when OD_{600nm} of the bacteria reached around 1. The whole-cell reaction mix was maintained at the same conditions for soluble intracellular extract-mediated reactions.

2.3. UV-Vis Spectroscopy

To observe the optical property of gold nanoparticles, samples from the reaction mix or supernatant after centrifugation at 3000 $\times g$ were analyzed using UV-vis spectroscopy (Genesys 10 S UV-Vis spectrophotometer; Fisher Scientific, Pittsburgh, PA, USA) operated at a resolution of 1 nm ranging from 200 to 800 nm at room temperature.

2.4. Collection of Nanoparticles

After 7 days of incubation in the presence of 2 mM HAuCl₄, the nanoparticles were first collected by centrifugation at 3000 $\times g$ for 5 min. The purpose of this low-speed centrifugation was to remove possible protein or other biological molecular precipitates after a week of incubation and acquire nanoparticles with minimum contamination of insoluble cellular components. The supernatant after low-speed centrifugation was further spun for 30 min at 17,000 $\times g$ to extract the remaining gold nanoparticles. After supernatant was carefully removed and the gold nanoparticles were dried at 37 $^{\circ}$ C in a drying oven (Isotemp™ General Purpose Heating and Drying Oven, Fisher Scientific, Pittsburgh, PA, USA). The dry weight of the nanoparticle pellet was measured and the gold nanoparticles were stored at -20° C. To collect the nanoparticles synthesized by whole cells, we centrifuged the reaction mix at 4500 $\times g$ for 15 min. Then, the pellets were resuspended in 8 M urea, sonicated and centrifuged to remove any soluble contents. The process was repeated three times and followed by two more washes with sterile deionized water. The samples were resuspended in sterile deionized water for electron microscopic analysis.

2.5. Characterization of Gold Nanoparticles Using Energy-Dispersive X-ray Spectroscopy and Transmission Electron Microscopy

We used transmission electron microscopy (TEM) to determine the morphological properties of the biologically synthesized gold nanoparticles and energy-dispersive X-ray spectroscopy (EDS) to identify the elemental composition of the nanoparticles. The samples for the TEM and EDS analysis were prepared similarly as described in Section 2.4 with some modifications at the end. The final gold nanoparticles were resuspended in sterile deionized water by sonication without the drying step.

An FEI Tecnai F30 super-twin field-emission-gun transmission electron microscope (TEM) (manufactured by the FEI Company in Hillsboro, OR, USA) operating at 300 kV was used to acquire the TEM images. A Hitachi HD2700 aberration-corrected scanning transmission electron microscope (manufactured by the Hitachi Company in Hillsboro in Chiyoda, Tokyo, Japan) was used to record the high-angle annular dark-field (HAADF) STEM images and to acquire the X-ray energy dispersive spectroscopy (EDS) spectra. The size of gold nanoparticles was analyzed using ImageJ Software.

2.6. Zeta Potential Analysis of Gold Nanoparticles

To estimate the stability of the nanoparticles, zeta potential of the gold nanoparticles generated by soluble extracts from the recombinant cells collected after high speed centrifugation was measured. The nanoparticles for zeta potential analysis were prepared in the same way as for TEM analysis. The nanoparticles were dispersed in sterile deionized water and zeta potential was recorded using Malvern Zetasizer Nano ZS system at pH of 6.48 and temperature of 25 °C (Particle Technology Labs, Downers Grove, IL 60515, USA).

2.7. Statistical Analysis

All data are expressed as mean \pm SD. Comparison between groups was evaluated with the Student *t* test. Probability values of <0.05 were considered significant.

3. Results

3.1. Expression of *R. tropici* Phytochelatin Synthase in *E. coli* DH5 α Cells

The expression of *R. tropici* phytochelatin synthase protein in *E. coli* was analyzed using SDS-PAGE. The soluble lysate of *E. coli* was separated by 10% SDS-PAGE gel and visualized using coomassie blue staining. Figure 1 shows that the intensity of a band with a size above 25 kD in the recombinant bacteria (pUC-Syn) was increased, compared to that of the endogenous band in the control cells (pUC19-Vec). The position of the band matched well with the predicted molecular weight of 28.95 kD of this protein [16]. Furthermore, we confirmed that the band did contain the *R. tropici* phytochelatin synthase using mass spectrum analysis in our previous study [16].

3.2. Synthesis and Yield of Nanoparticles by Soluble Intracellular Extracts

We reported that the recombinant *E. coli* cells showed faster growth under similar cultivation conditions, had stronger tolerance to heavy metal ions and an increased yield of selenium nanoparticles [16]. In this study, we revealed that the bacterial soluble extract-mediated reaction solution displayed a red wine color (Figure 2A,B), an indicator of successful gold nanoparticle synthesis [20,24]. To exclude the possibility that the intracellular contents could denature and precipitate during the 7-day reaction, creating a false increase in nanoparticle yield, we first centrifuged the reaction solution at $3000\times g$ for 5 min to remove possible precipitated biomolecules. After this low-speed centrifugation, the supernatant was clear but maintained the red color, implying that biomolecule precipitates were removed, but it still contained high level gold nanoparticles (Figures 2B and 3B). Further centrifugation of the supernatant shown in Figure 2B at $17,000\times g$ for 30 min allowed us to collect the remaining nanoparticles. In addition, the reaction containing intracellular extracts from pUC-Syn cells yielded a larger wet pellet than that of the control pUC19-Vec cells (Figure 2C). The dry weight of nanoparticle pellets synthesized by recom-

binant intracellular extracts and collected after low-speed isolation was greater, compared to the control group (3.5 ± 0.4 mg in pUC19-Vec vs. 5.9 ± 1.8 mg in pUC-Syn. Figure 2D). Importantly, the dry weight of the nanoparticles collected after high-speed centrifugation was also greater in pUC-Syn group (2.8 ± 0.6 mg in pUC19-Vec vs. 4.6 ± 1 mg in pUC-Syn. Figure 2D). Thus, our results identified that reaction using soluble intracellular extracts of the recombinant cells produced more gold nanoparticles, compared to those of the control cells.

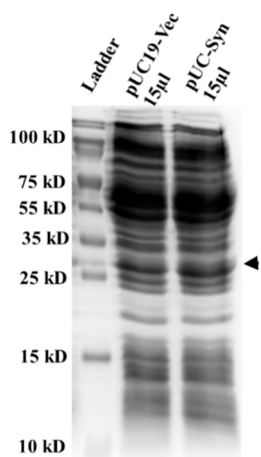


Figure 1. Expression of the phytochelatin synthase of *R. tropici*. in *E. coli*. 15 μ L of soluble cell lysate was run on 10% SDS PAGE gel and stained with commassie blue. Arrowhead indicates that pUC-Syn cells expressed phytochelatin synthase at the predicted molecular weight.

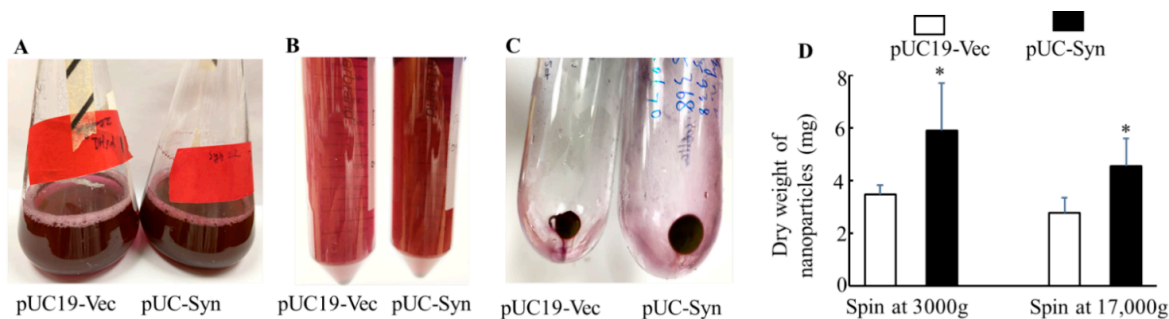


Figure 2. Synthesis and yield of gold nanoparticles by soluble intracellular extracts from bacteria. (A). Soluble intracellular reaction mix after 7 days of incubation with 2 mM HAuCl₄. (B). Supernatant collected after centrifugation of the reaction mix in A at 3000 g for 5 min. (C). Nanoparticle pellets obtained after further centrifuging the supernatant in (B) at 17,000 \times g. (D). Dry weight of nanoparticle pellets collected from 100 mL cell-free reaction mix after centrifugation at 3000 g and 17,000 g, respectively. $n = 4$. *: $p < 0.05$.

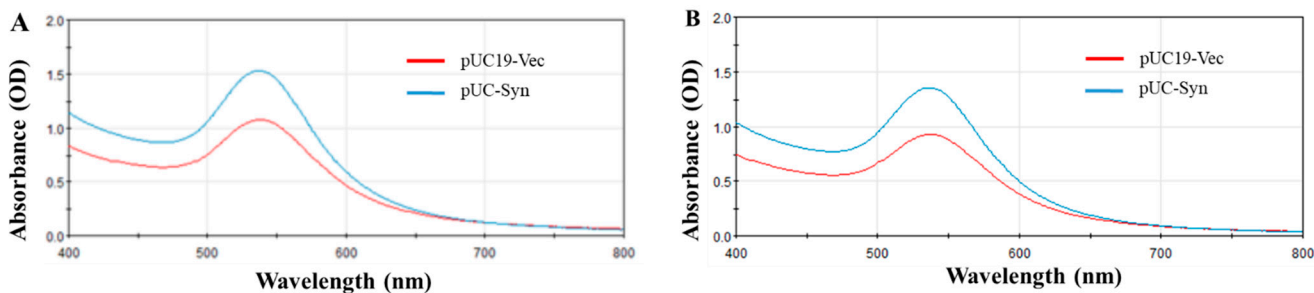


Figure 3. UV-vis spectra of nanoparticles. (A). UV-vis spectra of reaction mix containing soluble intracellular extracts before centrifugation. (B). UV-Vis spectra of supernatant collected after centrifugation of reaction mix at 3000 \times g for 5 min.

3.3. UV-Vis Spectral Characterization of Nanoparticles

UV-vis spectral analysis of the reaction mix before centrifugation or of the supernatant after centrifugation at $3000\times g$ detected an absorbance band between 500 and 600 nm in both pUC19-Vec and pUC-Syn cells (Figure 3A,B). The wavelength at which absorption maximum was observed was similar between the two groups, suggesting that the physical and chemical properties of the particles were probably similar (Figure 3A,B). The absorption peak of the reaction mix is consistent with what has been reported for gold nanoparticles with a small size and spherical shape [36,37]. However, the amplitude of the absorption maximum of the nanoparticles from pUC-Syn group was higher than that of the pUC19-Vec group (Figure 3A,B), indicating that there may be a higher density of gold nanoparticles in the reaction mediated by recombinant intracellular components, due to the formation of more gold nanoparticles. The UV-vis spectral results indicated that the low-speed centrifugation step might have helped improve the purity and quality of the nanoparticles, but at the cost of losing some nanoparticles. The absorption peak of the UV-Vis spectra was slightly reduced in both groups after low-speed centrifugation (Figure 3B).

3.4. Characterization of Gold Nanoparticles Using TEM

To characterize morphological properties of the nanoparticles, we examined the nanoparticles using TEM. The nanoparticles synthesized by extracellular method shared similar morphology and size among all groups (Figure 4A–F). The majority of the nanoparticles exhibited a sphere-like shape, while irregular-shape or cylindrical nanoparticles were also observed occasionally (marked by * in Figure 4A,B,D,E). The TEM images of nanoparticles under high resolution revealed more details on the nanoparticles' structures. Crystallographic planes of metal deposition could be seen in nanoparticles, and it appeared that the patterns of gold lattices were similar in nanoparticles made by soluble extracts from both cell groups (Figure 4C,F). The size of the nanoparticles from both groups varied within a similar range between 5–50 nm (Figure 4A,B,D,E, Table 1). Combination of the nanoparticles after low-speed and high-speed centrifugation didn't exhibit much difference in size between recombinant pUC-Syn and pUC19-Vec control cell group (26.06 ± 11.05 nm in pUC19-Vec vs. 26.63 ± 12.40 nm in pUC-Syn, $p > 0.05$, last two columns in Table 1). However, the low-speed centrifugation may help remove relatively larger nanoparticles and nanoparticle aggregates (Figure 4A,B and Figure 5B,C). This is more likely the case in recombinant cell group. The nanoparticles made by recombinant cellular extracts and collected after centrifugation at $3000\times g$ had a slightly but significantly larger size than those collected after centrifugation at $17,000\times g$ (Table 1). In general, the low-speed centrifugation at $3000\times g$ probably was not enough to separate nanoparticles ranging between 5–50 nm. In summary, while the extracellular synthesis method using soluble cellular extracts of recombinant cells produced more nanoparticles, the size, shapes and structure of these nanoparticles were not significantly different from those generated by the control pUC19-Vec cells.

Table 1. Comparison of nanoparticle size.

	D1 (pUC19-Vec Cell Group After Spin at 3000 g)	D2 (pUC19-Vec Cell Group After Spin at 17,000 g)	S1 (pUC-Syn Recombinant Cell Group After Spin at 3000 g)	S2 (pUC-Syn Recombinant Cell Group After Spin at 17,000 g)	D1 + D2	S1 + S2
Diameter (nm) (mean \pm SD)	26.49 ± 14.75	25.87 ± 8.95	28.95 ± 12.13	24.72 ± 12.30	26.06 ± 11.05	26.63 ± 12.40
Number of Nanoparticles	137	309	234	285	446	519
<i>p</i> value	D1 vs. D2, $p > 0.05$ D1 vs. S1, $p > 0.05$ D1 vs. S2, $p > 0.05$	D2 vs. D1, $p > 0.05$ D2 vs. S1, $p < 0.001$ D2 vs. S2, $p > 0.05$	S1 vs. D1, $p > 0.05$ S1 vs. D2, $p < 0.001$ S1 vs. S2, $p < 0.001$	S2 vs. D1, $p > 0.05$ S2 vs. D2, $p > 0.05$ S2 vs. S1, $p < 0.001$	D1+D2 vs. S1+S2, $p > 0.05$	D1+D2 vs. S1+S2, $p > 0.05$

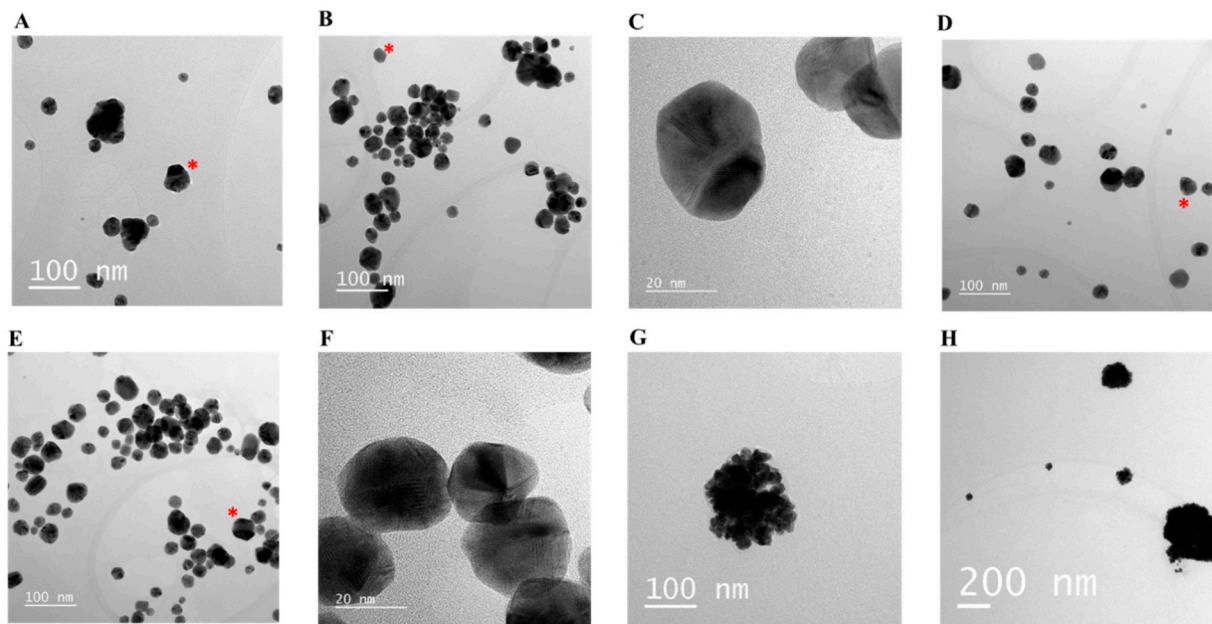


Figure 4. Structural analysis of nanoparticles by TEM. (A–C): TEM micrographs of nanoparticles synthesized by soluble extracts from pUC19-Vec cells collected after centrifugation at $3000\times g$ (A) and further at $17,000 g$ (B,C). (D–F): TEM micrographs of nanoparticles synthesized by soluble extracts from pUC-Syn cells collected after centrifugation at $3000\times g$ (D) and further at $17,000 g$ (E,F). (G,H): TEM micrographs of nanoparticles synthesized by pUC-Syn whole cells. * irregular-shape or cylindrical nanoparticles.

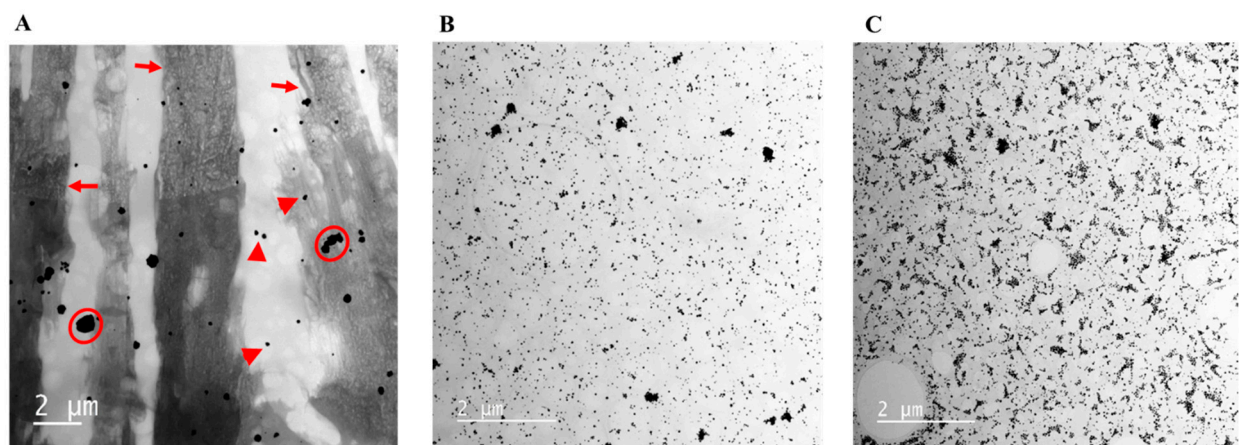


Figure 5. TEM images of nanoparticles synthesized by whole recombinant cells and soluble intracellular extracts of recombinant cells. (A). TEM micrograph of nanoparticles generated by whole cells. (B). TEM micrograph of nanoparticles synthesized by soluble extracts collected after centrifugation at $3000\times g$. (C). TEM micrographs of nanoparticles yielded by soluble extracts collected after further centrifugation at $17,000\times g$. Arrows indicate cellular debris; arrowheads indicate nanoparticles. Circles include large aggregates of nanoparticles.

Nevertheless, a comparison of the images of nanoparticles synthesized by whole cells and soluble intracellular extracts revealed some important differences, even if both reaction media were from recombinant bacteria. Firstly, and importantly, there was a large amount of cellular debris in the nanoparticle samples obtained by whole-cell reaction (Figure 5A), while the background of the images of the nanoparticles formed from soluble intracellular extract-mediated reaction was clear and lack of such cellular debris (Figure 5B,C). Secondly, the size and shape of the nanoparticles from whole-cell reaction and extracellular synthesis method were different. The nanoparticles generated by whole cell-mediated reaction had irregular shape and formed large aggregates (Figure 4E,F and Figure 5A). Thirdly, the

yield of nanoparticles by extracellular method was much higher than that of nanoparticles from whole cell-mediated reaction (Figure 5A–C). The nanoparticles shown in Figure 5A were isolated from a single 100 mL of whole cell reaction, while nanoparticles in B and C were collected from a single 100 mL of soluble intracellular extract-mediated reactions, and resuspended in the same final volume of deionized water for TEM analysis. Thus, the concentration of nanoparticles was an indicator of the nanoparticle yield, which suggested that the extracellular synthesis of gold nanoparticles was more efficient and had a higher yield of nanoparticles. Due to the low yield of nanoparticles by whole-cell reaction and formation of large nanoparticle aggregates, it was difficult to obtain enough images of individual nanoparticles for size measurement.

3.5. Compositional Analysis of Nanoparticles Using STEM and EDS

Since the nanoparticles synthesized by soluble intracellular extracts displayed similar physical characteristics, independent of cell type and centrifugation speed, we proposed that all of them should have similar elemental compositions. Thus, we only selected the nanoparticles obtained after high-speed centrifugation for compositional assessment using EDS coupled with STEM. Our results in Figure 6 demonstrated that the nanoparticles were indeed gold nanoparticles. Figure 6A shows the high-angle annular dark field (HAADF) micrograph of the gold nanoparticles synthesized by pUC19-Vec cells collected after centrifugation at $17,000\times g$. Figure 6B displays the color-coded EDS elemental map of the gold nanoparticles, and Figure 6C shows the spectra of EDS with energy peaks of mainly two elements, gold and copper, in the nanoparticle sample; Figure 6C–F shows similar results for the gold nanoparticles synthesized by the pUC-Syn recombinant cells. The signals of copper in Figure 6C,F arose from the TEM grid that supported the nanoparticles. The energy peak of aluminum in Figure 6 F was from contamination during the preparation of the STEM sample. These results demonstrated that gold was the only element detected in the nanoparticles. Therefore, the extracellular method using soluble intracellular extracts successfully generated gold nanoparticles.

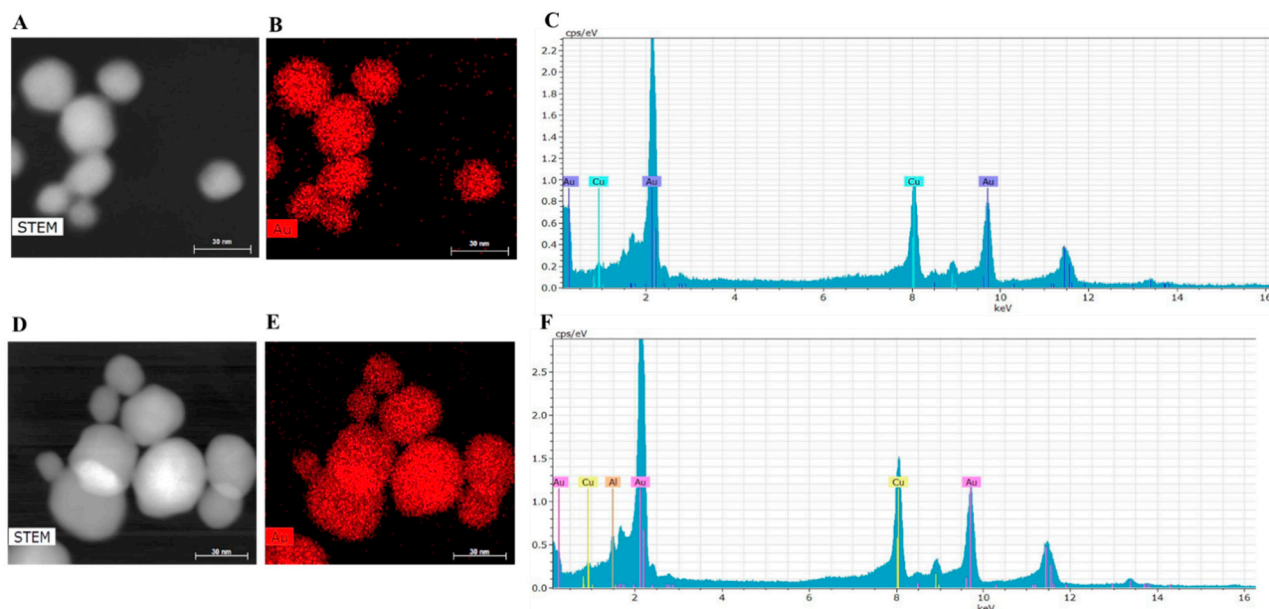


Figure 6. STEM scanning and EDS compositional analysis of gold nanoparticles. (A). HAADF STEM micrograph of gold nanoparticles synthesized by pUC19-Vec cells collected after centrifugation at $17,000\times g$. (B). Color-coded EDS elemental map of the gold nanoparticles. (C). EDS spectrum of gold nanoparticles showing the energy peaks of different elements. (D–F) show the same analysis used in (A–C), but of gold nanoparticles from pUC-Syn recombinant cells.

3.6. Measurement of Zeta Potential of Gold Nanoparticles

Zeta potential measurement can assess the surface charges of nanoparticles and estimate the degree of repulsion between the charged particles in colloid status. A zeta potential lower than -30 mV or higher than $+30$ mV usually suggests good colloid stability of nanoparticles due to the electrostatic repulsion between individual particles [38]. In this study, zeta potential was determined using Malvern Zetasizer Nano ZS system (Particle Technology Labs, Downers Grove, IL 60515, USA). Since the TEM and EDS analysis identified that nanoparticles produced by recombinant and control soluble intracellular extracts had similar physical properties, we only measured the zeta potential of nanoparticles from recombinant cells. When the nanoparticles were dispersed in deionized water at 25 °C and a pH of 6.48, two peaks were identified. Peak one had an average of -41.5 ± 6.92 mV, and its area contributed to 98% of the potential distributions. The average zeta potential of peak two was 21.8 ± 2.72 mV; however, it only accounted for 2% of the potential distributions (Figure 7). The average zeta potential of all the analyzed nanoparticles was 41.2 ± 7.29 mV (Figure 7). These results indicated that the gold nanoparticles synthesized by the soluble extracts from recombinant *E. coli* cells were very stable.

		Mean (mV)	Area (%)	St Dev (mV)
Zeta potential (mV): -41.2	Peak 1	-41.5	98	6.92
Zeta Deviation (mV): 7.29	Peak 2	-21.8	2.0	2.72
Conductivity (mS/cm): 0.00916	Peak 3	0.00	0.0	0.00

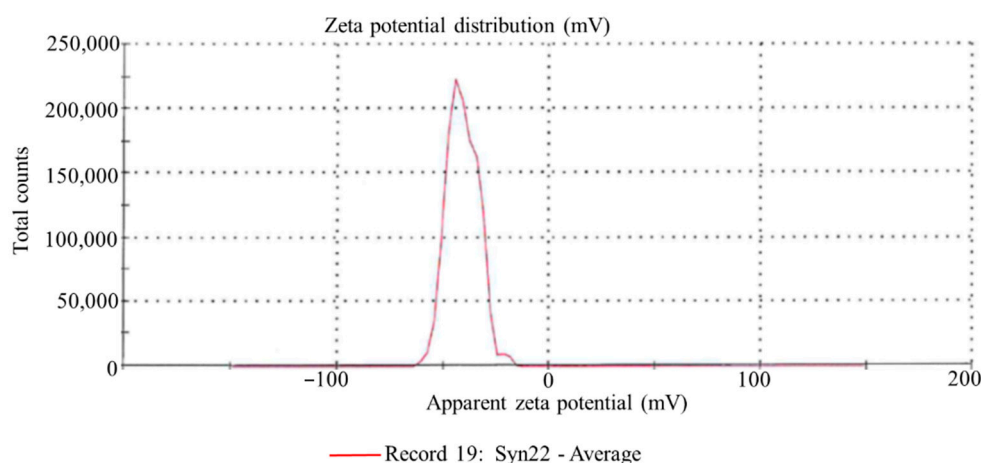


Figure 7. Zeta potential analysis of gold nanoparticles. Zeta potential distribution of gold nanoparticles synthesized by soluble extracts from recombinant *E. coli* cells.

4. Discussion

Herein, we tested the capacity of the soluble intracellular extracts from *E. coli* cells as reaction media to synthesize gold nanoparticles. We revealed that the soluble intracellular extracts were able to synthesize gold nanoparticles with a spherical shape and a size ranging from 5 to 50 nm (Figure 2A,B Figure 3A,B, Figures 4 and 6, Table 1). Notably, the yield of gold nanoparticles produced by reaction containing soluble components from recombinant cells transformed with *R. tropici* phytochelatin synthase was increased by more than 60%, compared to that from the cells only transformed with empty plasmid vector (Figure 2C,D).

Phytochelatin, the enzymatic products of phytochelatin synthase, are small soluble peptides that play an essential role in resisting heavy metal toxicity in plants [8–11]. Their potential role in nanoparticle synthesis has been reported [13–16]. In the present study, we proposed that the overexpression of the enzyme promoted the synthesis of phytochelatin in the host *E. coli* cells based on literature review and our own observations, although we

didn't measure the phytochelatin synthase activity or the level of phytochelatin in the cells. It was recently found out that the prokaryotic phytochelatin synthase in cyanobacterium *Geitlerinema* sp. showed basal phytochelatin synthesis activity [7]. Importantly, its activity was further enhanced when the cyanobacterium *Geitlerinema* sp. were exposed to cadmium as evidenced by the increase in the production of phytochelatin in these cells [7]. We also reported that the recombinant *E. coli* cells transformed with *R. tropici* phytochelatin synthase gene displayed a better basal growth and an enhanced tolerance to a few heavy metals [16], indicating that the enzyme was active and generated phytochelatin that facilitate the survival of host cells upon heavy metal challenges. Thus, we believe that the soluble extracts of these recombinant cells should contain a higher level of phytochelatin, which played an important role in improving the capacity of nanoparticle synthesis when only intracellular extracts were used as reaction media (Figure 2C,D). Since the repeats of glutamate and cysteine in phytochelatin usually are no more than 5, which give a molecular weight less than 3 kD; therefore, the increase in these short peptides most likely enhanced the reduction of gold ions, according to a recent report showing that the molecules smaller than 3 kD were able to reduce gold ions [19].

Many other cellular components, such as enzymes, functional groups of proteins, and amino acids, are involved in the reduction of metal ions, nucleation, growth, capping and stabilization of gold nanoparticles [19,24–32,39]. Therefore, a faster growth resulting in yield of a greater cell mass and a larger amount of cellular components further augmented the efficiency of nanoparticle production mediated by cell-free intracellular contents.

While overexpression of phytochelatin synthase enhanced gold nanoparticle synthesis, the physical and chemical properties of these nanoparticles synthesized by soluble intracellular extracts from either recombinant cells or control cells were not significantly different (Figure 3A,B and Figure 4, Table 1). The size variation and morphology of these nanoparticles were largely similar. Particularly, the nanoparticles showed very similar pattern of gold lattices in high-resolution images obtained by TEM (Figure 4C,F). These revelations implied that the mechanism and pathway of nanoparticle formation could be the same in the two cell groups when soluble intracellular extracts were used as reaction media, since the physical and chemical properties of biologically synthesized nanoparticles are largely determined by the components of the reaction solution and the reaction conditions to form nanoparticles [19,39].

The extracellular synthesis platform using soluble intracellular extracts not only successfully produced gold nanoparticles, but also aided in removing the cellular debris encountered in whole-cell synthesis. TEM images of nanoparticles uncovered many large insoluble fragments of cellular debris in the nanoparticle samples synthesized by whole-cell method (Figure 5A), which were not seen in the images of nanoparticles made by extracellular method (Figure 5B,C). One of the challenges to the application of bacteria for producing nanoparticles in large quantity and pure form is the isolation of nanoparticles from insoluble cellular components. Thus, our findings suggested that extracellular synthesis of nanoparticles is a promising platform to produce pure nanoparticles for their diverse applications. Engineering *E. coli* cells so that they carry critical components for successful formation of different nanoparticles has the potential to enable *E. coli* to serve as a platform for production of various nanoparticles.

Furthermore, it is interesting that the whole-cell method appeared to also have a lower capacity to synthesize gold nanoparticles. The gold nanoparticles and nanoparticle aggregates were sparsely dispersed among debris (Figure 5A). The difference in morphology, size and yield between nanoparticles produced by whole cells and soluble intracellular components indicated that they have used a different mechanism to form gold nanoparticles. The pathway and mechanism of gold nanoparticle formation in both cases are not clear and need further investigations.

Gold nanoparticles have the potential for application in many aspects of nanotechnology; for an example, serving as vehicles for drug delivery, production of materials for photothermal conversion in light therapy, development of diagnostic instruments, cancer

treatment, antibacterial agents in infection control, as well as building blocks for nano-electronics, colorimetric sensing, surface-enhanced Raman scattering (SERS) and localized surface plasmon resonance (LSPR) [33,40–42]. An important prerequisite for these applications is that the nanoparticles should be stable in colloidal status, since aggregation of the nanoparticles will significantly impair their behavior and functional activity. Measurement of zeta potential of the extracellular method synthesized gold nanoparticles suggested that these nanoparticles had relatively high stability (Figure 7), which will allow us to further pursue their applications, particularly in biological systems.

5. Conclusions

In summary, we demonstrated that overexpression of a prokaryotic phytochelatin synthase in *E. coli* improved the efficiency of extracellular gold nanoparticle synthesis mediated by soluble cellular extracts. Moreover, the extracellular nanoparticle synthesis platform helped omit the separation of nanoparticles from cellular debris when whole cells are used as nanoparticle biofactories. Our results suggested that genetic modification of bacteria that carry essential components in pathways of nanoparticle formation may help expand the extracellular method to produce diverse nanoparticles in large quantity for their applications in nanotechnology.

Author Contributions: Q.Y., designed the experiments, assembled genes, produced the engineered bacteria, synthesized gold nanoparticles, analyzed the data and wrote the manuscript. Z.X., characterized the NPs, analyzed data and contributed to writing the manuscript. M.B., performed UV-vis to analyze the absorption of NP samples and reviewed the manuscript. All authors have read and agreed to the published version of the manuscript.

Funding: This study was supported by funding from DoD/ARO (award number: W911NF1810444).

Institutional Review Board Statement: Not applicable.

Informed Consent Statement: Not applicable.

Data Availability Statement: Data are available to audience.

Acknowledgments: The research is supported by DoD/ARO under Grant No. W911NF-18-1-0444. Research carried out in part at the Center for Functional Nanomaterials, Brookhaven National Laboratory, which is supported by the U.S. Department of Energy, Office of Basic Energy Sciences, under Contract No. DE-SC00112704. The authors greatly appreciate Yong Ding at George Institute of Technology for his help in performing the TEM, STEM and EDS examinations.

Conflicts of Interest: The authors declared no conflict of interest.

References

1. Khan, I.; Saeed, K.; Khan, I. Nanoparticles: Properties, applications and toxicities. *Arab. J. Chem.* **2019**, *12*, 908–931. [[CrossRef](#)]
2. Lloyd, J.R. Microbial reduction of metals and radionuclides. *FEMS Microbiol. Rev.* **2003**, *27*, 411–425. [[CrossRef](#)]
3. Singh, P.; Kim, Y.J.; Zhang, D.; Yang, D.C. Biological synthesis of nanoparticles from plants and microorganisms. *Trends Biotechnol.* **2016**, *34*, 588–599. [[CrossRef](#)]
4. Grill, E.; Winnacker, E.-L.; Zenk, M.H. Phytochelatins, a class of heavy-metal-binding peptides from plants, are functionally analogous to metallothioneins. *Proc. Natl. Acad. Sci. USA* **1987**, *84*, 439–443. [[CrossRef](#)] [[PubMed](#)]
5. Grill, E.; Loffer, S.; Winnacker, E.L.; Zenk, M.H. Phytochelatins, the heavy-metal-binding peptides of plants, are synthesized from glutathione by a specific γ -glutamylcysteine dipeptidyl transpeptidase (phytochelatin synthase). *Proc. Natl. Acad. Sci. USA* **1989**, *86*, 6838–6842. [[CrossRef](#)] [[PubMed](#)]
6. Tsuji, N.; Nishikori, S.; Iwabe, O.; Shiraki, K.; Miyasaka, H.; Takagi, M.; Hirata, K.; Miyamoto, K. Characterization of phytochelatin synthase-like protein encoded by alr0975 from a prokaryote, *Nostoc* sp. PCC 7120. *Biochem. Biophys. Res. Commun.* **2004**, *315*, 751–755. [[CrossRef](#)] [[PubMed](#)]
7. Bellini, E.; Varotto, C.; Borsò, M.; Rugnini, L.; Bruno, L.; Di Toppi, L.S. Eukaryotic and Prokaryotic Phytochelatin Synthases Differ Less in Functional Terms Than Previously Thought: A Comparative Analysis of *Marchantia polymorpha* and *Geitlerinema* sp. PCC 7407. *Plants* **2020**, *9*, 914. [[CrossRef](#)] [[PubMed](#)]
8. Cobbett, C.; Goldsbrough, P. Phytochelatins and Metallothioneins: Roles in Heavy Metal Detoxification and Homeostasis. *Annu. Rev. Plant Biol.* **2002**, *53*, 159–182. [[CrossRef](#)]

9. Emamverdian, A.; Ding, Y.; Mokhberdoran, F.; Xie, Y. Heavy metal stress and some mechanisms of plant defense response. *Sci. World J.* **2015**, *2015*, 1–18. [[CrossRef](#)]
10. Gupta, D.K.; Huang, H.G.; Corpas, F.J. Lead tolerance in plants: Strategies for phytoremediation. *Environ. Sci. Pollut. Res.* **2013**, *20*, 2150–2161. [[CrossRef](#)] [[PubMed](#)]
11. Cobbett, C. Phytochelatins and Their Roles in Heavy Metal Detoxification. *Plant Physiol.* **2000**, *123*, 825–832. [[CrossRef](#)]
12. Tennstedt, P.; Peisker, D.; Böttcher, C.; Trampczynska, A.; Clemens, S. Phytochelatin Synthesis Is Essential for the Detoxification of Excess Zinc and Contributes Significantly to the Accumulation of Zinc. *Plant Physiol.* **2009**, *149*, 938–948. [[CrossRef](#)] [[PubMed](#)]
13. Choia, Y.; Park, T.J.; Lee, D.C.; Lee, S.Y. Recombinant *Escherichia coli* as a biofactory for various single- and multi-element nanomaterials. *Proc. Natl. Acad. Sci. USA* **2018**, *115*, 5944–5949. [[CrossRef](#)]
14. Zhang, D.; Yamamoto, T.; Tang, D.; Kato, Y.; Horiuchi, S.; Ogawa, S.; Yoshimura, E.; Suzuki, M. Enhanced Biosynthesis of CdS Nanoparticles Through *Arabidopsis Thaliana* Phytochelatin Synthase-Modified *Escherichia Coli* with Fluorescence Effect in Detection of Pyrogallol and Gallic Acid. *Talanta* **2019**, *195*, 447–455. [[CrossRef](#)]
15. Zhang, D.; Tang, D.; Yamamoto, T.; Kato, Y.; Horiuchi, S.; Ogawa, S.; Yoshimura, E.; Suzuki, M. Improving Biosynthesis of AuPd Core-Shell Nanoparticles Through *Escherichia Coli* with the Assistance of Phytochelatin for Catalytic Enhanced Chemiluminescence and Benzyl Alcohol Oxidation. *J. Inorg. Biochem.* **2019**, *199*, 110795. [[CrossRef](#)]
16. Yuan, Q.; Bomma, M.; Hill, H.; Xiao, Z. Expression of Rhizobium tropici phytochelatin synthase in *Escherichia coli* resulted in increased bacterial selenium nanoparticle synthesis. *J. Nanoparticle Res.* **2020**, *22*, 1–13. [[CrossRef](#)]
17. Singh, H.; Du, J.; Singh, P.; Yi, T.H. Extracellular synthesis of silver nanoparticles by *Pseudomonas* sp. THG-LS1.4 and their antimicrobial application. *J. Pharm. Anal.* **2018**, *8*, 258–264. [[CrossRef](#)] [[PubMed](#)]
18. Vetchinkina, E.; Loshchinina, E.; Kupryashina, M.; Burov, A.; Pylaev, T.; Nikitina, V. Green synthesis of nanoparticles with extracellular and intracellular extracts of basidiomycetes. *PeerJ* **2018**, *6*, e5237. [[CrossRef](#)]
19. Molnár, Z.; Bóday, V.; Szakacs, G.; Erdélyi, B.; Fogarassy, Z.; Sáfrán, G.; Varga, T.; Kónya, Z.; Tóth-Szeles, E.; Szűcs, R.; et al. Green synthesis of gold nanoparticles by thermophilic filamentous fungi. *Sci. Rep.* **2018**, *8*, 3943. [[CrossRef](#)]
20. Camas, M.; Camas, A.S.; Kyeremeh, K. Extracellular Synthesis and Characterization of Gold Nanoparticles Using *Mycobacterium* sp. BRS2A-AR2 Isolated from the Aerial Roots of the Ghanaian Mangrove Plant, *Rhizophora racemosa*. *Indian J. Microbiol.* **2018**, *58*, 214–221. [[CrossRef](#)]
21. Li, X.; Xu, H.; Chen, Z.S.; Chen, G. Biosynthesis of Nanoparticles by Microorganisms and Their Applications. *J. Nanomater.* **2011**, *2011*, 270974. [[CrossRef](#)]
22. Sharma, D.; Kanchi, S.; Bisetty, K. Biogenic synthesis of nanoparticles: A review. *Arab. J. Chem.* **2019**, *12*, 3576–3600. [[CrossRef](#)]
23. Vaidyanathan, R.; Gopalram, S.; Kalishwaralal, K.; Deepak, V.; Pandian, S.R.; Gurunathan, S. Enhanced silver nanoparticle synthesis by optimization of nitrate reductase activity. *Colloids Surf. B Biointerfaces* **2010**, *75*, 335–341. [[CrossRef](#)]
24. Leng, Y.; Fu, L.; Ye, L.; Li, B.; Xu, X.; Xing, X.; He, J.; Song, Y.; Leng, C.; Guo, Y.; et al. Protein-directed synthesis of highly monodispersed, spherical gold nanoparticles and their applications in multidimensional sensing. *Sci. Rep.* **2016**, *6*, 28900. [[CrossRef](#)]
25. Ravindra, P. Protein-mediated synthesis of gold nanoparticles. *Mater. Sci. Eng. B* **2009**, *163*, 93–98. [[CrossRef](#)]
26. Engelbrekt, C.; Sørensen, K.H.; Zhang, J.; Welinder, A.C.; Jensen, P.S.; Ulstrup, J. Green synthesis of gold nanoparticles with starch–glucose and application in bioelectrochemistry. *J. Mater. Chem.* **2009**, *19*, 7839–7847. [[CrossRef](#)]
27. Tajammul Hussain, S.; Iqbal, M.; Mazhar, M. Size control synthesis of starch capped-gold nanoparticles. *J. Nanoparticle Res.* **2009**, *11*, 1383–1391. [[CrossRef](#)]
28. Xiao, Y.; Pavlov, V.; Levine, S.; Niazov, T.; Markovitch, G.; Willner, I. Catalytic growth of Au nanoparticles by NAD(P)H cofactors: Optical sensors for NAD(P)+-dependent biocatalyzed transformations. *Angew. Chem. Int. Ed.* **2004**, *43*, 4519–4522. [[CrossRef](#)] [[PubMed](#)]
29. Liu, J.; Qin, G.; Raveendran, P.; Ikushima, Y. Facile “green” synthesis, characterization, and catalytic function of beta-D-glucose-stabilized Au nanocrystals. *Chemistry* **2006**, *12*, 2131–2138. [[CrossRef](#)] [[PubMed](#)]
30. Maruyama, T.; Fujimoto, Y.; Maekawa, T. Synthesis of gold nanoparticles using various amino acids. *J. Colloid Interface Sci.* **2015**, *447*, 254–257. [[CrossRef](#)]
31. Wangoo, N.; Bhasin, K.K.; Mehta, S.K.; Suri, C.R. Synthesis and capping of water-dispersed gold nanoparticles by an amino acid: Bioconjugation and binding studies. *J. Colloid Interface Sci.* **2008**, *323*, 247–254. [[CrossRef](#)]
32. Bhattacharjee, R.R.; Das, A.K.; Haldar, D.; Si, S.; Banerjee, A.; Mandal, T.K. Peptide-assisted synthesis of gold nanoparticles and their self-assembly. *J. Nanosci. Nanotechnol.* **2005**, *5*, 1141–1147. [[CrossRef](#)]
33. Hu, X.; Zhang, Y.; Ding, T.; Liu, J.; Zhao, H. Multifunctional Gold Nanoparticles: A Novel Nanomaterial for Various Medical Applications and Biological Activities. *Front. Bioeng. Biotechnol.* **2020**, *8*, 990. [[CrossRef](#)]
34. Marsic, D.; Hughes, R.C.; Byrne-Steele, M.L.; Ng, J.D. PCR-based gene synthesis to produce recombinant proteins for crystallization. *BMC Biotechnol.* **2008**, *8*, 44. [[CrossRef](#)] [[PubMed](#)]
35. Yuan, Q.; Bomma, M.; Xiao, Z. Enhanced Silver Nanoparticle Synthesis by *Escherichia Coli* Transformed with *Candida Albicans* Metallothionein Gene. *Materials* **2019**, *12*, 4180. [[CrossRef](#)] [[PubMed](#)]
36. Martínez, J.C.; Chequer, N.A.; González, J.L.; Cordova, T. Alternative Methodology for Gold Nanoparticles Diameter Characterization Using PCA Technique and UV-VIS Spectrophotometry. *Nanosci. Nanotechnol.* **2012**, *2*, 184–189. [[CrossRef](#)]

37. Tang, J.; Gao, K.; Ou, Q.; Fu, X.; Man, S.Q.; Guo, J.; Liu, Y. Calculation extinction cross sections and molar attenuation coefficient of small gold nanoparticles and experimental observation of their UV–vis spectral properties. *Spectrochim. Acta Part A Mol. Biomol. Spectrosc.* **2018**, *191*, 513–520. [[CrossRef](#)]
38. Bhattacharjee, S. DLS and zeta potential—What they are and what they are not? *J. Control. Release* **2016**, *235*, 337–351. [[CrossRef](#)] [[PubMed](#)]
39. Shedbalkar, U.; Richa, S.; Sweetey, W.; Sharvari, G.; Chopade, B.A. Microbial synthesis of gold nanoparticles: Current status and future prospects. *Adv. Colloid Interface Sci.* **2014**, *209*, 40–48. [[CrossRef](#)] [[PubMed](#)]
40. Homberger, M.; Simon, U. On the application potential of gold nanoparticles in nanoelectronics and biomedicine. *Philos. Trans. R. Soc. A Math. Phys. Eng. Sci.* **2010**, *368*, 1405–1453. [[CrossRef](#)]
41. Hu, M.; Chen, J.; Li, Z.Y.; Au, L.; Hartland, G.V.; Li, X.; Marquez, M.; Xia, Y. Gold nanostructures: Engineering their plasmonic properties for biomedical applications. *Chem. Soc. Rev.* **2006**, *35*, 1084–1094. [[CrossRef](#)] [[PubMed](#)]
42. Lee, J.-H.; Cho, H.-Y.; Choi, H.K.; Lee, J.-Y.; Choi, J.-W. Application of Gold Nanoparticle to Plasmonic Biosensors. *Int. J. Mol. Sci.* **2018**, *19*, 2021. [[CrossRef](#)] [[PubMed](#)]